JOURNAL OF MODERN OPTICS, 1998, VOL. 45, NO. 8, 1613–1627

Hollow waveguide integrated optics: a novel approach to 10 μm laser radar

R. M. JENKINS, R. W. J. DEVEREUX and A. F. BLOCKLEY

Lasers and Photonics Department, Defence Evaluation and Research Agency, Room PA109, St Andrews Road, Malvern, Worcestershire, WR14 3PS England

(*Received 3 February 1998*)

Abstract. A novel integrated optic approach to the manufacture of 10.6 μm coherent laser radar systems is described and demonstrated. The approach uses hollow waveguides to guide light between system components which are integrated into a common substrate. The design, manufacture and operation of a seven-element subsystem which is compact and rugged and provides a mixing efficiency in excess of 80% of the theoretical maximum are discussed. The demonstration of the subsystem as a simple homodyne vibrometer is also outlined.

1. Introduction

Coherent continuous-wave (CW) 10.6 μm laser radar systems are typically based on the use of CW CO_2 waveguide lasers in conjunction with a range of other passive and active components, including beam splitters, Brewster plates, waveplates, lenses, detectors and modulators [1]. In practice these components have to be very accurately aligned with respect to one another in order to form a transmit–receive interferometer which can provide efficient homodyne–heterodyne detection. The conventional approach to building such systems is to hold the individual components on mounts having multiaxial tilt and translation facilities. Elaborate manual techniques are then used to align the components with respect to one another. The approach leads to systems which are bulky, which are often lacking in stability and which are difficult and costly to manufacture.

This paper describes an integrated optics approach to the manufacture of such systems. The approach is based on the use of hollow waveguides to guide light between components located in a common dielectric substrate. Both the hollow waveguides and the alignment slots that the components are located in, are formed within the surface of the substrate using computer numerical control (CNC) machining techniques. The concept, referred to as hollow waveguide integrated optics (HOW-IO), has the potential to reduce size, to increase ruggedness, to simplify manufacture and to lower manufacturing costs. The guidance of light from one component to another also leads to inherent advantages in relation to the practical problems of achieving and maintaining good coherent mixing efficiencies. A schematic diagram of a HOW-IO subsystem based on a design used in earlier work at our laboratory is illustrated in figure 1 [1]. As illustrated in the figure, in conjunction with a laser source, some transmit–receive optics and a detector, the subsystem becomes a complete single-aperture monostatic laser radar.

0950–0340/98 $12·00

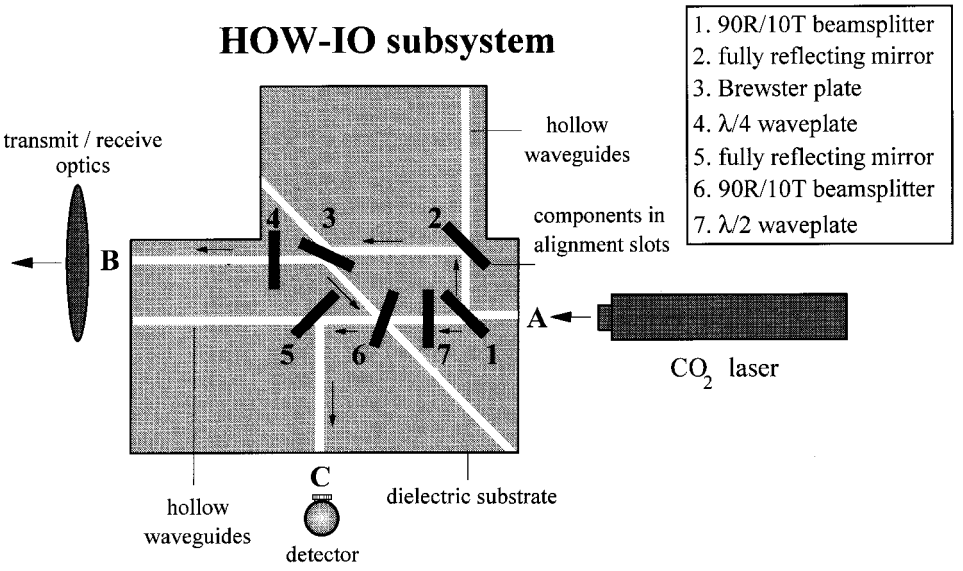

Figure 1. Schematic diagram of the HOW-IO subsystem whose design, manufacture and assessment are described in the paper. The diagram illustrates its use in conjunction with a laser source, some transmit–receive optics and a detector.

In the rest of the paper the design, manufacture, and operation of a HOW-IO subsystem of the form illustrated in figure 1 are described. In section 2 the detailed operation of the subsystem is discussed. The underlying hollow waveguide mode theory and the implications for HOW-IO system design are outlined in section 3. The manufacture and optical assessment of the subsystem are reviewed in section 4. In section 5, measurements of coherent mixing efficiency are described and analysed together with a demonstration of the subsystem as a simple vibrometer. Finally, in section 6 the plans for further work are summarized.

2. Subsystem operation

Before entering into the detail of the HOW-IO implementation of the subsystem its operation is first clarified. The subsystem allows three separate optical functions to be realized: firstly the main portion of the prime laser source is effectively transmitted to the target through path A–1–2–3–4–B, secondly the return from the target is effectively coupled to the detector via route B–4–3–6–5–C and thirdly a small portion of the prime laser source is split off to act as the local oscillator field via A–1–7–6–5–C. In conjunction with the Brewster plate 3, the quarter-wave plate 4 allows the transmit–receive function to be realized with a single-aperture system. In this context, the half-wave plate 7 allows the p polarized input to be converted to an s-polarized field. This ensures efficient mixing of the local oscillator field with the received field following its reflection from Brewster plate 3.

Although values of 90% reflection–10% transmission have been chosen for both beam splitters 1 and 6, this choice of reflect-to-transmit ratio was selected for our experimental demonstration of the HOW-IO concept rather than being the ideal

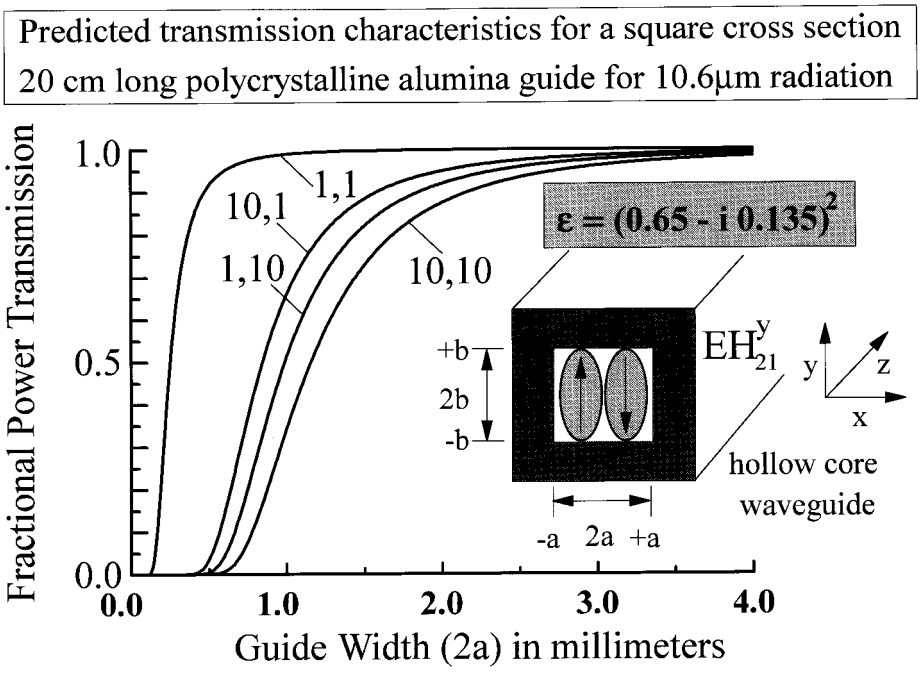

Figure 2. Predictions of fractional power transmission as a function guide width for a hollow polycrystalline alumina waveguide 20 cm long. The predictions are undertaken for a range of EH_{pq} modes. The inset clarifies the nature of the guide and mode nomenclature. All calculations are for 10.6 μm radiation.

ratio for a real laser radar system. In practice the values of these two beam splitters dictate the percentage of injected laser beam power which reaches the detector as a local oscillator signal. Typically, optimum detector performance is achieved with a local oscillator power level of a milliwatt or less [2]. With a laser source providing 1.0 W of CW power, beam splitters 1 and 6 would be required to have a *combined* transmission of 0.1% (i.e. 99.9% reflection–0.1% transmission) in order to provide 1.0 mW of local oscillator power. This could be achieved with both beam splitters having 3.0% transmission–97% reflection.

3. Hollow waveguide mode propagation theory and design criteria

From the perspective of optical field propagation, the HOW-IO subsystem illustrated in figure 1 can be viewed as a series of short lengths of hollow square-section linear waveguide, coupled together by reflective or transmissive components. In order to develop design criteria for HOW-IO systems the underlying waveguide mode propagation theory is first reviewed. The inset in figure 2 illustrates a rectangular cross-section hollow waveguide of height $2a$ and width $2b$ surrounded by a homogeneous dielectric material of complex dielectric constant ε. With its time dependence omitted, to a first approximation, the propagation of the EH_{pq}^{th} waveguide mode along the z axis can be described by the normalized electric field expression [3, 4]

$$E_{pq}(x,y,z) = \begin{cases} \dfrac{1}{(ab)^{1/2}} \cos\left(p\dfrac{\pi x}{2a}\right) \cos\left(q\dfrac{\pi y}{2b}\right) \exp\left(-\gamma_{pq} z\right) \text{ for } p,q \text{ odd}, \\ \dfrac{1}{(ab)^{1/2}} \sin\left(p\dfrac{\pi x}{2a}\right) \sin\left(q\dfrac{\pi y}{2b}\right) \exp\left(-\gamma_{pq} z\right) \text{ for } p,q \text{ even}. \end{cases} \quad (1)$$

Here, p and q are the mode indices relating to the field dependencies along the x and y axes respectively. γ_{pq} is the propagation constant of the mode and is defined by the expression.

$$\gamma_{pq} = \alpha_{pq} - \mathrm{i}\beta_{pq}. \quad (2)$$

α_{pq} and β_{pq} are the attenuation and phase coefficients respectively of the mode. These in turn are given by

$$\alpha^{y}_{pq} = \frac{\lambda^2}{16}\left[\frac{p^2}{a^3}\,\mathrm{Re}\left(\frac{1}{(\varepsilon-1)^{1/2}}\right) + \frac{q^2}{b^3}\,\mathrm{Re}\left(\frac{\varepsilon}{(\varepsilon-1)^{1.2}}\right)\right] \quad (3)$$

and

$$\beta_{pq} = \frac{2\pi}{\lambda} - \frac{\pi\lambda}{16}\left[\left(\frac{p}{a}\right)^2 + \left(\frac{q}{b}\right)^2\right]. \quad (4)$$

The y superscript on the attenuation coefficient in equation (3) relates to the fact that this expression is for the y polarized EH_{pq} mode. This nomenclature is clarified in the inset to figure 2.

By suitable choice of wall material, attenuated internal reflection phenomena analogous to those at the heart of step index solid core waveguides and fibres can be beneficially brought into play with respect to achieving suitably low fundamental mode attention coefficients [5]. In relation to equation (3), this amounts to choosing wall materials having optical properties which result in the magnitudes of the real parts of the complex dielectric constant terms being minimized. However, from this viewpoint, even with some of the better polycrystalline wall materials such as BeO or Al_2O_3, the waveguides are still inherently much more lossy in nature than are their solid core counterparts. Nevertheless, low attenuation coefficients can still be achieved in practice by making the guide width large compared with the propagating wavelength and hence making the magnitudes of the λ^2/a^3 and λ^2/b^3 terms in equation (3) very small; clearly, for square guides $a = b$.

In order to put this conclusion on a firmer footing the fractional power transmission $T = \exp(-2\alpha^{y}_{pq}L)$ is plotted for a wavelength of 10.6 μm and for guide widths in the range 0.0–4.0 mm in figure 2. The predictions are for a hollow waveguide of square cross-section and 20 cm long, formed in polycrystalline alumina. The calculations are based on the use of equation (3) in conjunction with a value for the complex dielectric constant $\varepsilon = (0.65\text{–}\mathrm{i}0.135)^2$. This was calculated from broad spectrum reflectivity measurements for a 99.5% pure polycrystalline alumina that we have used in earlier work. The value is in good agreement with the results given by Khelkhal and Herlemont [6] for a similar type of alumina. The plots are made for the modes EH^{y}_{11} (1, 1), $EH^{y}_{1\,10}$ (1, 10), $EH^{y}_{10\,1}$ (10, 1) and $EH^{y}_{10\,10}$ (10, 10). Very high fundamental mode power transmission is predicted for guide widths of a millimetre or more. For guides greater than 4.0 m in width the range of higher-order modes also exhibit very low attenuation. Because the effective complex dielectric constant varies with the exact composition

and nature of the type of polycrystalline alumina utilized, the results can only provide a useful guideline of what may be anticipated. In more general terms, polycrystalline alumina is an attractive material for HOW-IO systems for similar reasons to its choice as the basis of CO_2 waveguide lasers; it is a rugged machinable ceramic with a good thermal conductivity and a low coefficient of linear thermal expansion. Furthermore, unlike beryllia (BeO), which in some respects is a better option, it is non-toxic.

From the viewpoint of creating hollow waveguide systems in a polycrystalline alumina substrate, the results in figure 2 suggest that a waveguide width of a millimetre or more would be perfectly acceptable in terms of achieving high fundamental mode transmission even for systems with quite long waveguide paths. In this context the fractional power transmission through a path made up of n 20 cm lengths is simply $T_{\text{total}} = (T_{20})^n$, where T_{20} is the fractional transmission for a single guide 20 cm long. Unfortunately, the provision of low attenuation coefficients is not the only factor that has to be taken into account in terms of ensuring efficient fundamental mode propagation through the waveguide system. Misalignment at the points where one waveguide is coupled to another via an integrated transmissive or reflective component can cause light to be coupled into higher-order modes in the receiving waveguide at the expense of fundamental mode coupling. This is a consequence of field mismatch caused either by amplitude distortion produced by lateral misalignment or by phase mismatch produced by angular misalignment. Combinations of the different forms of misalignment are also possible. For systems based on a guide 1.0 mm wide, as illustrated in figure 2, high-order modes are more heavily attenuated than the fundamental mode; as a result the power transmission through the system could be significantly reduced by misalignment. However, with waveguide widths of 3.0 mm or more, the attenuation coefficients of quite high-order modes are themselves quite small; as such, the deleterious impact of misalignment on overall power transmission can be circumvented. At first sight this would appear to be a useful solution to the problem; however, higher-order mode excitation produced by misalignment is detrimental to system performance for two additional reasons: firstly, at exit aperture B, whereas the fundamental waveguide mode couples about 98% of its power to the TEM_{00} free-space Hermite–Gaussian mode [4], higher-order waveguide modes couple to high-order free-space modes and reduce the effectiveness with which power can be directed at a target; secondly, because of the power orthogonal nature of the waveguide modes, only the interference of like modes produce power modulation at the detector; as such the fundamental mode fidelity achieved in both the local oscillator and the target return paths has a major impact on the coherent detection efficiency (the mixing efficiency) that can be achieved.

In practice, higher-order mode excitation needs to be avoided in order that overall system performance is not compromised as a consequence of reduced power transmission, coupling to high-order free-space modes or poor mixing efficiency. In this respect, overlap integral calculations based on the field expression in equations (1)–(4) were undertaken in relation to defining the alignment tolerances that would be necessary in order to achieve fundamental mode coupling coefficients of suitably large magnitude at the waveguide-to-waveguide interfaces. The results indicate that angular and lateral alignment tolerances of $\pm\lambda/10a$ and $\pm a/10$ respectively provide fundamental mode power-coupling efficiencies (one

waveguide to another) in excess of 95%. It should be noted that these tolerances are complementary. The smaller the guide width, the easier the angular alignment tolerance becomes at the expense of a tighter lateral alignment tolerance and vice versa. On the basis of these considerations the original aim was to base practical systems on waveguides 1.0 mm wide. This equated to a guide half-width $a = 0.5$ mm and led to angular and lateral alignment tolerances of ± 2.0 mrad and ± 0.05 mm respectively. However, waveguide manufacturing tests based on the use of an appropriately milling bit led to major problems with tool wear and damage in the course of the CNC machining process. Ultimately a guide width of 2.0 mm became a practical compromise. Even though this led to the need for a tighter angular alignment tolerance of ± 1.0 mrad it resulted in much more consistent manufacture of waveguide circuits.

It is worth noting that the effective $1/e^2$ beam diameter in a 2.0 mm waveguide is 1.4 mm (e.g. 2.0 mm $\times$ 0.7 [4]). This is a factor of four smaller than that established at the field mixing point in the free-space laser radar system on which the HOW-IO design was based [1]. This has the practical consequence that the angular alignment tolerance necessary for a given mixing efficiency will be a factor of four less demanding in the hollow waveguide system. Additionally, angular misalignment does not lead to lateral beam offset, and angular misalignments are compounded in a less detrimental manner in HOW-IO systems. As such they have the potential to out-perform their free-space counterparts in terms of optical mixing efficiency. The possibilities for reducing the required angular alignment tolerances in HOW-IO systems even further by the realization of systems based on smaller waveguide dimensions is also an attractive option.

4. Hollow waveguide integrated optics subsystem manufacture and optical assessment

A HOW-IO subsystem of the form illustrated schematically in figure 1 was manufactured in a polycrystalline alumina (Kyocera A479) substrate utilizing CNC milling techniques. The machining process firstly involved the creation of the alignment slots for the location of the optical components. The slots were designed for components which were 20.0 mm square and 4.0 mm thick. The channels of 2.0 mm square cross-section which provide the basis for the interconnecting waveguides were formed between the alignment slots in a secondary milling operation. Machining tolerances were dictated by the design criteria developed in the previous section. In practice these equated to achieving lateral alignment accuracies between waveguides and components of ± 0.1 mm ($\pm a/10$), and angular alignment accuracies between waveguides and reflective components of ± 0.5 mrad (the effect of reflection led to the angular alignment tolerance being tightened to $\pm \lambda/20a$).

The required angular alignment tolerance also dictated the accuracy with which the width of a given alignment slot was made with respect to the thickness of the related reflective component. This was the most demanding aspect of the machining work. The need to maintain appropriate angular alignment tolerances also imposed a limit on the parallelism of transmissive components. The required parallelism was dependent on the angular orientation and the refractive index of the component. For the ZnSe Brewster plate in the subsystem this equated to the need for a parallelism better than 40 s, which is easily achieved in practice.

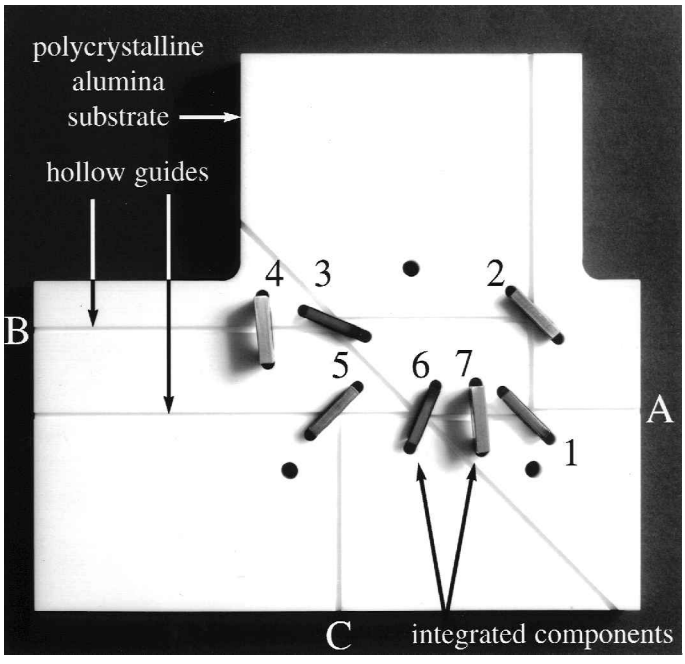

Figure 3. Plan-view photograph of the HOW-IO subsystem, illustrating the waveguide network and the seven integrated components in the polycrystalline alumina substrate. The three through-holes allow the polycrystalline alumina lid, which forms the fourth wall of all the waveguides, to be fixed to the substrate.

With the machined polycrystalline substrate in hand, completion of the system manufacture merely involved the location of the components in the appropriate alignment slots. A photograph showing a plan view of the resulting 180 mm × 190 mm × 20 mm HOW-IO subsystem with all its integrated components in position is shown in figure 3. In relation to identifying the waveguides and integrated components, figure 1 provides a useful cross-reference. The three holes which are clearly visible in the surface of the substrate pass all the way through it, facilitating its fixing, together with a polycrystalline alumina lid which forms the fourth wall of all the waveguides, to a metal baseplate. A number of the waveguides are extended in length beyond that required for guiding the light between the circuit of components. These extra lengths of waveguide are important for alignment and optical assessment procedures. When complete confidence in the machining and assembly techniques is established, and the laser source itself is integrated into the substrate, extended waveguides will not be required. As indicated by the tight packing density achieved with the actual circuit of components, the area and weight of the substrate can then be significantly reduced.

The optical characteristics of the completed subsystem were assessed with an experimental configuration analogous to that illustrated in figure 1. The measurements were based on the use of a conventional free-space CO_2 laser source (Edinburgh Instruments PL2). This was grating tuned and optogalvanically stabilized to provide output on the P20 transition at 10.6 μm. The horizontally polarized output was spatially filtered before being coupled into the waveguide

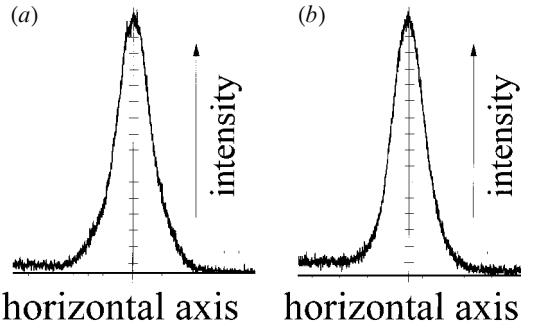

Figure 4. Beam profiles measured at waveguide exit aperture C with a 'scanning slit' profiler (BeamScan 2180) following propagation through (*a*) the complete transmit–receive path and (*b*) the local oscillator path. Both profiles are of reasonable fundamental mode form.

structure by means of an appropriate lens. With the aim of ensuring that efficient fundamental mode excitation was established in the input guide at aperture A, three practical guidelines were adhered to: firstly the establishment of a TEM_{00} beam waist of diameter $0.7 \times 2a$ (1.4 mm) at A; secondly the lateral alignment of the beam axis and the guide axis to $\pm a/10$ (± 0.1 mm); thirdly the angular alignment of the beam axis and the guide axis to $\pm \lambda/10a$ (± 1.0 mrad). The establishment of these alignment criteria should lead to about 90% of the power in the TEM_{00} beam being coupled to the fundamental waveguide mode.

In order to check the alignment of the laser beam with respect to the input guide at aperture A, the output from waveguide aperture B was monitored utilizing a 'scanning slit' beam profiler (BeamScan 2180). Fine adjustments to the overall alignment of the structure were then made whilst checking the profile in order to ensure that efficient fundamental mode excitation was achieved. With this situation established, the beam profiles produced in propagation through the whole waveguide system were measured. Figure 4 (*a*) illustrates the beam profile measured at exit aperture C as a result of the input beam propagating through the complete transmit–receive leg A to C via components 1, 2, 3, 4, external mirror, 4, 3, 6 and 5, and figure 4 (*b*) that through the local oscillator leg A to C via components 1, 7, 6 and 5. In addition to the measurements of transmitted beam profiles, power transmission from the input beam at aperture A to apertures B and C was also recorded. The results are as follows: B, 79.7%; C, 71.5% (all components in transmit–receive path plus external mirror at B); C, 0.49% (all components in local oscillator path). The errors in all measurements were of the order of $\pm 1.0\%$ of the measured values.

As noted above, the beam profile and power transmission measurements through the complete transmit–receive path required the use of a well aligned, fully reflecting mirror at aperture B in order to return the fundamental mode field to the waveguide structure. This again required an angular alignment tolerance of the order of ± 0.5 mrad. In relation to maximizing the power transmission through the transmit–receive path the correct orientation of the quarter-wave plate was of paramount importance. This was achieved by adjusting its orientation until the power transmission from A to C, via this path, was maximized. Under this condition a double pass through the wave plate causes the light to become linearly

polarized orthogonal to the plane of the substrate; as a consequence its reflection from the Brewster plate is maximized. This is exactly the function required with respect to a field transmitted to, and received from, a target.

The measured values of power transmission are in good agreement with the data provided by the optical component manufacturers and the predicted waveguide attenuation. With the external, fully reflecting mirror in position, the predicted transmission through the nine-element transmit–receive path A to C was 71.85%. This took into account an initial aperture loss. By comparison the measured value of transmission was 71.5%.

5. Measurement of mixing efficiency and demonstration as a vibrometer

Although the beam profile and power transmission measurements provided a good indication that the waveguides and integrated components were aligned to a high degree of accuracy, measurement of the mixing efficiency provided a quantitative assessment of the subsystem. This involved the use of an external mirror at aperture B mounted on a piezoelectric transducer (PZT) element. This allowed optical path modulation, and hence a phase modulation, to be imposed on the fundamental mode field returned to the waveguide structure. Following its return path to the detector via components 4, 3, 6 and 5, the phase-modulated field was mixed with the local oscillator field which reaches the detector via components 1, 7, 6 and 5. When the phase-modulated field interferes with the local oscillator field on the surface of the detector a power modulation is produced.

We now consider this situation in more detail in order to see how the magnitude of the resulting power modulation is directly related to the mode fidelity that has been achieved in the local oscillator and transmit–receive arms of the subsystem respectively. Assume that in the plane of the detector ($z = 0$) the local oscillator field consists solely of the spatial model EH_{pq} having complex amplitude $A_{pq} \exp(\mathrm{i}\alpha_{pq})$. Now, suppose that this is mixed with the field returned to the detector along the transmit–receive path via the external mirror. Assume that in the plane of the detector this field also consists solely of the waveguide mode EH_{rs} having a complex amplitude $B_{rs} \exp(\mathrm{i}\beta_{rs})$. In addition, we infer that owing to the axial motion of the external mirror this field is also phase modulated as a function of time, with a modulation function of the form $2\pi ft$, where f is the modulation frequency. The resultant time-dependent field intensity pattern in the x–y plane of the detector due to the interference of the modes EH_{pq} and EH_{rs}, is given by

$$I(x,y,t) = [A_{pq}E_{pq}(x,y)]^2 + [B_{rs}E_{rs}(x,y)]^2 + 2A_{pq}E_{pq}(x,y)B_{rs}E_{rs}(x,y) \times \cos[\alpha_{pq} - (\beta_{rs} + 2\pi ft)]. \tag{5}$$

Integration of $I(x,y,t)$ across the x–y plane allows the time dependent power falling on the detector to be predicted as

$$P(t) = \int\int I(x,y,t)\,\mathrm{d}x\,\mathrm{d}y = A_{pq}^2 + B_{rs}^2 + 2A_{pq}B_{rs}\cos[\alpha_{pq} - (\beta_{rs} + 2\pi ft)] \times \int\int E_{pq}(x,y)E_{rs}(x,y)\,\mathrm{d}x\;\mathrm{d}y. \tag{6}$$

Because of the power orthogonal nature of the modes, consideration of equation (6) leads to the conclusion that the value of the third term is zero unless the local oscillator mode $EH_{rs}(x, y)$ interferes with an identical transverse mode in the field returned to the detector via the transmit–receive path, that is if $p = r$ and $q = s$. Under this condition the resultant power modulation as a function of time is given by

$$P_{pq}(t) = A_{pq}^2 + B_{pq}^2 + 2A_{pq}B_{pq}\cos[\alpha_{pq} - (\beta_{pq} + 2\pi ft)]. \tag{7}$$

In the idealized case where both the received and the local oscillator fields reaching the detector via the relevant waveguide paths are of pure fundamental mode form, $p = q = 1$, the peak-to-peak value of the modulation characteristic is given by

$$P_{11_{pk\text{-}pk}} = 4A_{11}B_{11}. \tag{8}$$

Values for A_{11} and B_{11} can be deduced from measurements of the power transmitted through the local oscillator and transmit–receive paths. Substitution in equation (8) makes it possible to predict a value for $P_{pk\text{-}pk}$. This predicted value is a theoretical maximum because it is based on the assumption that the measured powers relate to fields of pure fundamental mode form. In practice, because of misalignments which result in power being coupled to higher-order modes, the measured value of $P_{pk\text{-}pk}$ will be lower. The ratio of the measured value to the theoretical maximum is the mixing efficiency of the system. The mixing efficiency is a quantitative measure of the alignment accuracy that has been achieved.

Firstly, in order to ascertain that the PZT was operating properly and that power modulation could be achieved, the output from waveguide aperture C was measured on a 4.0 mm square $Hg_{1-x}Cd_xTe$ detector as a triangular drive signal was applied to it. The resulting drive and detector traces are shown in figure 5.

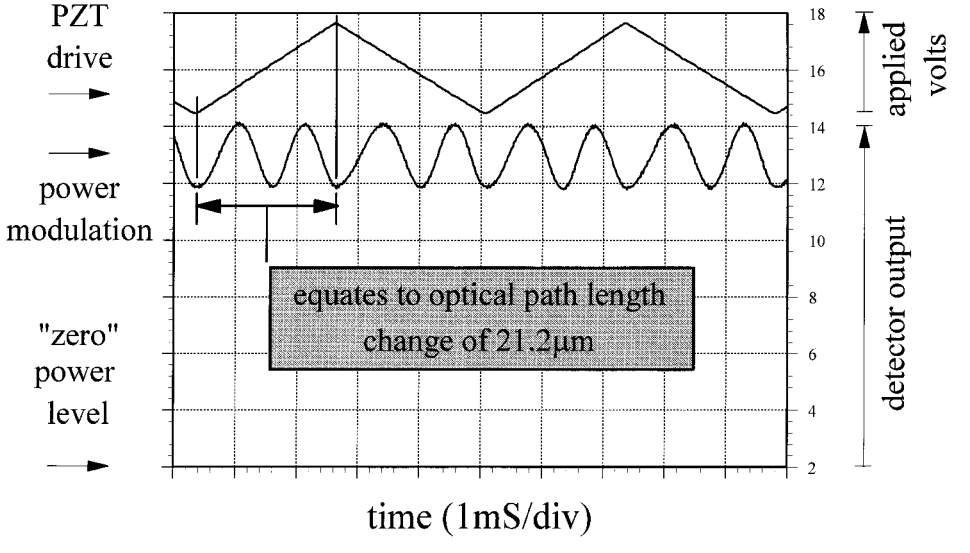

Figure 5. Oscilloscope traces of the triangular drive signal applied to the PZT on which the fully reflecting mirror at aperture B is mounted, and the resulting power modulation characteristic measured on the $Hg_{1-x}Cd_xTe$ detector at aperture C.

They illustrate that within the limits of the drive signal two complete cycles of the interference characteristic are swept out. This indicates the PZT element is producing a total round-trip optical path change (to the external mirror and back) of 21.2 μm, that is a total axial motion of the order of 10.6 μm. The approximately sinusoidal power modulation that is produced rides on a larger dc power level; the oscilloscope was adjusted so that the zero power axis coincided with the lowest oscilloscope graticule. By analogy with the earlier discussions about the orientation of the quarter-wave plate, the orientation of the half-wave plate in the local oscillator path is of critical importance in maximizing the efficiency with which the fields in the local oscillator and transmit–receive path are mixed. In order that optimum performance was achieved, the orientation of the half-wave plate was adjusted whilst the magnitude of the interference signal was monitored.

With the orientation of the half-wave plate optimized, the peak-to-peak value of the modulation characteristics represented approximately 20% of the dc value. In order to assess accurately the mixing efficiency, measurements of the absolute powers in the local oscillator and transmit–receive paths were undertaken with a thermopile power meter placed at waveguide aperture C. The measurement for a given path was achieved with the other blocked off. With an input beam power of 105.00 mW, the measured value of the output power from the local oscillator path was 0.51 mW, and from the transmit–receive path 75.06 mW. The moduli of the fundamental mode fields in the local oscillator and transmit–receive paths are then $0.71\,\mathrm{mW}^{1/2}$ and $8.6\,\mathrm{mW}^{1/2}$ respectively. Substitution of these values in equation (8) allows us to predict the theoretical maximum for the peak-to-peak magnitude $P_{pk\text{-}pk}$ of the interference characteristic as $4 \times 0.71 \times 8.66 = 24.59\,\mathrm{mW}$.

The measured value of the peak-to-peak magnitude of the power modulation was made by manually adjusting the voltage applied to the piezoelectric element. This was done in an incremental manner in order to ascertain accurately the maximum and minimum value of power output in terms of the readings taken from the thermopile power meter. With an input beam power level of 105.00 mW the maximum value was measured as 82.83 mw, and the minimum as 62.81 mW. Thus $P_{\max} - P_{\min} = P_{pk\text{-}pk} = 20.02\,\mathrm{mW}$. Comparison with the predicted value leads to the conclusion that the system provides a mixing efficiency which is 81.4% of the theoretical maximum.

The result suggests that the waveguide structure and the integrated components were very well aligned with respect to one another. The fact that the measured value of the mixing efficiency was not even closer to the theoretical maximum was the consequence of a number of factors. Firstly, the alignment tolerances that had been aimed for and achieved in the subsystem would not, in themselves, have facilitated pure fundamental mode propagation. Even if this had been the case, the fundamental mode transmission fidelity would be impaired by a number of other factors, including imperfections in the TEM_{00} input beam; misalignment of the input beam with respect to the input waveguide; diffraction effects in the fundamental mode transmission through the transmitting components during which the beam is unguided; asymmetric diffraction in relation to reflection from, or transmission through, components which are obliquely oriented with respect to the waveguide axis. Small inaccuracies in the orientations of the $\lambda/2$ and $\lambda/4$ wave plates could also have a large impact on the mixing efficiency that was achieved in practice.

In the context of the mixing efficiency measurements, an additional source of potential error occurs as a result of the assumptions upon which the measurements, and the ensuing calculations, are themselves based. In the theoretical analysis, because in practice the fundamental mode dominates in both the transmit–receive and the local oscillator paths, we assumed that this is the only mode that needs to be considered as far as the power modulation characteristic is concerned. However, all modes in the local oscillator and transmit–receive fields will contribute to the interference signal. Thus, the instantaneous power on the detector is from equation (7),

$$\sum_{p=1}^{\infty}\sum_{q=1}^{\infty} P_{pq}(t)$$

In turn, the resultant power modulation characteristic is the sum of the individual components each with its appropriate magnitude and phase.

It is impossible to predict or measure accurately the mode spectra in the local oscillator and transmit–receive fields at the detector plane. However, it is unlikely that complex amplitudes of the mode spectra produced there will be similar, let alone identical. This is a consequence of the different nature of the components and the misalignments in each path and of the different lengths of the paths themselves. With respect to the former, angular misalignments can result in the excitation of higher-order modes which are either $\pi/2$ rad or $3\pi/2$ rad out of phase with the fundamental depending just on the sense of the tilt. The latter point about the path lengths is also salient. As an example, consider the situation where angular misalignment of the input beam results in the modes EH_{12} and EH_{13} being excited in the input guide at aperture A in addition to the fundamental. From equation (4) it is possible to show that, following propagation through a path length L, the phase difference between the fundamental mode and the mode EH_{pq} is given by

$$\phi_{11-pq} = L\frac{\pi\lambda}{16a^2}[(p^2-1)+(q^2-1)]. \tag{9}$$

From input aperture A to the beam recombiner 6 the transmit–receive and local oscillator paths differ in length by about 250 mm. As a consequence when the fundamental mode fields in each path are in phase at the beam recombiner, the EH_{12} mode components will, from equation (9), have a phase difference of about 1.6 rad while the EH_{13} mode components will have a phase difference of about 4.2 rad. This highlights the fact that significant phase differences can be produced between the propagating modes just as a result of the path differences themselves.

Because of the diverse nature of the magnitudes and senses of the misalignments that will exist in practice, and the different path lengths between their sources and the beam recombiner 6, we feel justified in proposing that averaging effects come into play. These are such that, when a certain higher-order mode is contributing to the fundamental mode interference characteristic in a manner which would cause an increase in the peak-to-peak value of the power modulation produced on the detector, another is likely to be contributing in negative manner. Furthermore, with the amplitudes of the higher-order modes themselves being small, the magnitude of the product term in equation (8) will be even smaller, and the overall impact on the fundamental mode characteristics will be negligible.

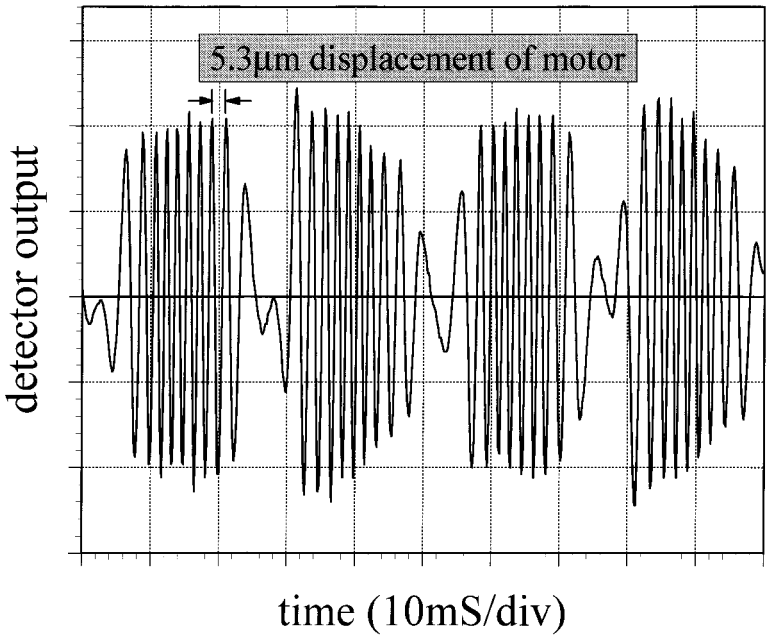

Figure 6. Vibrational signature of a dc electric motor measured with the HOW-IO subsystem in conjunction with a CO laser source, some transmit–receive optics and a $Hg_{1-x}Cd_xTe$ detector. The simple harmonic motion of the vibration is clear from the velocity variations in the signature.

Finally, in order to prove the operational potential of the HOW-IO subsystem an experimental configuration analogous to that illustrated in figure 1 was set up. A small electric motor held in a retort stand 5 m from the subsystem was used as a vibrating target. The field returned from the target was mixed with the local oscillator field on a cooled $Hg_{1-x}Cd_xTe$ detector positioned at exit aperture C. As the electric motor vibrated in its stand the optical path difference between it and the subsystem structure varied. This produced a phase modulation of the field returned to the detector and in turn produced power modulation on interference with the local oscillator field. An oscilloscope trace of the resulting detector output is illustrated in figure 6. Some consideration of the varying temporal separation between the peaks in the interference signal reveals that the motor is oscillating in its mount in a simple harmonic manner.

6. Conclusions and future work

In conclusion a seven-element HOW-IO subsystem has been designed, manufactured and optically assessed. The functionality of the subsystem replicates the transmit–receive interferometer at the heart of many coherent laser radar systems. As such it provides a useful demonstration of the state of the art of HOW-IO technology. The results of the optical assessments of the subsystem, including measurements of the mixing efficiency and vibrational signatures from laboratory targets, indicate that overall alignment accuracies of better than 80% of the theoretical maximum have been achieved in practice. The results prove that the

HOW-IO concept can be successfully applied to the realization of quite complex laser radar systems. They also highlight the advantages in the HOW-IO approach which make them far less susceptible than free-space systems to the effects of misalignment.

The practical value of the HOW-IO subsystem is currently being assessed in more detail in relation to its use for atmospheric wind measurements; direct comparisons with the performance of conventional free-space systems are also planned. In the next phase of work on the underlying technology the potential for integrating a CO_2 waveguide laser into the subsystem will be investigated. Both hybrid and monolithic integration approaches will be considered. This work will lead a step closer to the ultimate goal of realizing full integrated HOW-IO systems in which both passive and active components are integrated into the same dielectric substrate. The only external component would be the large-aperture secondary optic of the transmit–receive telescope. If successful, the HOW-IO approach should lead to a new generation of 10.6 μm laser radar systems which are rugged, compact and inexpensive to manufacture. The inherent advantages of guiding light between the components should also lead to systems having improved coherent detection performance compared with their free-space counterparts.

Because of the broad-waveband high-power transmission characteristics of suitably designed hollow waveguides, the underlying HOW-IO concepts should be applicable at other wavelengths and to other types of optical system. The use of the approach in the manufacture of widely used interferometer configurations (e.g. the Michelson interferometer) would seem logical. In more general terms some of the important field splitting and mixing functions that are necessary in HOW-IO systems could be achieved with the hollow waveguide analogues of the free-space components. Symmetric and asymmetric splitters [7–9] and coherent mixers [10] based on multimode interference concepts have already been demonstrated in practice with appropriately designed hollow waveguide structures. In principle these could lead to all-hollow waveguide systems which are cheap to produce and have very high power-handling characteristics. In the context of reducing costs and creating the potential for mass production, the development of lithographic and etching techniques analogous to those utilized in the semiconductor industry is also being considered. In this respect the use of different types of substrate material will also be investigated.

Acknowledgments

The authors would like to express their heartfelt appreciation to the following people: Mr Ken Huetson and Mr Jim Taylor of Shanock Precision Engineering and the staff at R. L. Smith Ltd for their excellent ceramic machining work, without which the concept could not have come to fruition; Mr Jim Redding† for his technical input and his enthusiasm about the concept; Mr John Quarrell† for his devoted work on engineering drawings for HOW-IO systems; Dr David Willetts†, Dr Michael Vaughan† and Mr Ben (R.) Foord† for encouragement and support in relation to more recent work on the feedthrough of HOW-IO technology into real laser radar systems. The authors are also indebted to Dr Michael Vaughan† for the stimulus that he provided during the process of getting

† All of the Defence Evaluation and Research Agency, Malvern.

the paper written and his useful suggestions about the draft manuscript. Likewise they would like to thank Dr Michael Harris† for constructive comments on the manuscript and valuable discussions about the section on the potential errors in the mixing efficiency measurements.

References

[1] Foord, R., Jones, R., Vaughan, J. M., and Willetts, D. V., 1983, *Appl. Optics*, **22,** 3787.
[2] Holmes, J. F., and Rask, B. J., 1995, *Appl. Optics*, **34,** 927.
[3] Krammer, H., 1976, *IEEE Jl quant. Electron*, **12,** 505.
[4] Laakmann, K. D., and Steier, W. H., 1976, *Appl. Optics*, **15,** 1334.
[5] Jenkins, R. M., and Devereux, R. W. J., 1985, *IEEE J quant. Electron.* **21,** 1722.
[6] Khelkhal, , and Herelemont, 1992, *Appl. Optics*, **31,** 4175.
[7] Jenkins, R. M., and Heaton, J. M., 1991, *Int. Pat. Applic.* PCT/GB91/02129, filed 2 December 1991, UK Pat. Priority Date, 20 December 1990.
[8] Jenkins, R. M., Devereux, R. W. J., and Heaton, J. M., 1992, *Optics Lett.*, **17,** 991.
[9] Jenkins, R. M., 1991, Int. Pat. Applic. PCT/GB91/02131, filed 2 December 1992, UK Pat. Priority Date 20 December 1990.
[10] Jenkins, R. M., Devereux, R. W. J., and Heaton, J. M., 1994, *Optics Commun.*, **110,** 410.